DOI 10.5012/bkcs.2011.32.5.1715

Synthesis of Nanoporous Structured SnO_2 and its Photocatalytic Ability for Bisphenol A Destruction

Jieun Kim, Jun Sung Lee, and Misook Kang*

Department of Chemistry, College of Science, Yeungnam University, Gyeongsan, Gyeongbuk 712-749, Korea
**E-mail: mskang@ynu.ac.kr*
Received September 8, 2010, Accepted March 21, 2011

Nanoporous structured tin dioxide (SnO_2) is characterized and its application in the photocatalytic destruction of endocrine, Bisphenol A, is examined. Transmission electron microscopy (TEM) reveals irregularly shaped nanopores of size 2.0-4.5 nm. This corresponds to the result of an average nanopore distribution of 4.5 nm, as determined by Barret-Joyner-Halenda (BJH) plot from the isotherm curve. The photoluminescence (PL) curve, corresponding to the recombination between electron and hole, largely decreases in the TiO_2/nanoporous SnO_2 composite. Finally, a synergy effect between TiO_2 and porous SnO_2 is exhibited in photocatalysis: the photocatalytic destruction of Bisphenol A is improved by combining the nanoporous structured SnO_2 with TiO_2, and 75% decomposition of 10.0 ppm of Bisphenol A is achieved after 24 h.

Key Words : Nanoporous structured SnO_2, Photocatalytic destruction, Bisphenol A, BJH plot

Introduction

Many studies have been conducted on the photocatalytic treatment of environmental pollutants using semiconductors such as TiO_2.[1-5] However, the applications of nanosized TiO_2 or nanosized metal/TiO_2 have been limited for industrial use because of poor performances. Furthermore, the anatase structural limitation has been suggested, and so the expending toward the introduction of new structural titanium frameworks needs. Meanwhile recent research has focused intensively on nanoporous particles. Nanoporous photocatalysis offers the following advantages: 1) the formation of ultra fine titania particles; 2) increased adsorption; 3) higher acidity, which enhances electron abstraction; and 4) less UV-light scattering. We also previously reported[6] the synthesis of high-concentration, titanium-incorporated nanoporous silicates (Ti-NPS) and their photocatalytic performance for toluene oxidation: the photocatalytic decomposition for toluene was enhanced by 50% in Ti-NPS. In particular, the initial performance for toluene removal, which was attributed to the adsorption ability of nanopores, was higher than that with nonporous titania photocatalyst. However, the advantage of using a regular porous structure in the gaseous system was not clearly identified. In addition, little research has been conducted to investigate the photocatalysis of nanoporous SnO_2 and TiO_2 composites. In particular, the photocatalytic activity on Sn-TiO_2 composites has recently attracted attention for methylene blue and RhB dye degradation compared to pure TiO_2 under UV light. A coupled TiO_2-SnO_2 photocatalyst has been reported to work efficiently.[7] Although the band gap energy of SnO_2 (3.8 eV) is higher than that of TiO_2 (3.2 eV), the conduction band of SnO_2 is at a lower level (conduction band of 0.25 V *vs*. NHE at pH 7 than that of TiO_2 (conduction band of 0.5 V *vs*. NHE at pH 7. Because of this potential difference, the photo-excited electrons can easily migrate to the conduction band of SnO_2 from TiO_2 and enhance the photocatalytic activity. Therefore, in this study, the role of nanoporous SnO_2 particles in a photocatalytic system for the destruction of endocrine, Bisphenol A, is investigated. This study focuses on the synthesis and characterization of nanoporous structured SnO_2, which is applied to photocatalysis. Nanoporous structured SnO_2 was produced using an NPS framework, prepared by a conventional hydrothermal method, as a template. As a comparative material, nanosized SnO_2 was synthesized by hydrothermal method.

Experimental

Synthesis of Nanoporous Structured SnO_2. The general preparation method of nanoporous silicates (MCM-41) by hydrothermal method has been reported elsewhere.[8-10] Nanoporous structured tin dioxide (SnO_2) was produced using an NPS framework as a template. As a Sn source, 0.1 mol of amorphous SnO_2 prepared by sol-gel method was added to 100 mL of distilled water and then stirred until the solution became homogeneous. A solution including 1.0 g of NPS (MCM-41), which was prepared using a conventional hydrothermal method, was dropped slowly into the former solution to serve as a template for the nanopores. Crystallization was performed at room temperature for 24 h, and the resulting powder was washed, filtered, and calcined at 500 °C for 3 h in air. The final powder was treated with a 10 wt % HF solution to remove the silicate component in the nanoporous framework, and finally washed with distilled water until pH=7 and dried again. Additionally, nanosized SnO_2 was synthesized by hydrothermal method and thermally treated at 500 °C for 3 h in air for use as a comparison material. For application to the photodestruction of 2-chlorophenol, the 1.0 wt % TiO_2 (sol-gel method, anatase

structure, 50-70 nm): 1.0 wt % nanosized or nanoporous SnO_2 was mixed in DI water solvent, stirred and thermally treated at low temperature of 150 °C for 1 h to depress its sintering at high temperature.

Characterization. The synthesized, nanosized and nanoporous structured SnO_2 powder was subjected to X-ray diffraction (XRD, Rigaku, D/MAX-1200) with nickel-filtered CuKα radiation (30 kV, 30 mA) at angles from 10 to 80° 2θ, and from 1 to 10°. The pore sizes and shapes of the nanosized and nanoporous structured SnO_2 powders were determined by transmission electron microscopy (TEM, H-7600, Hitachi, Japan)/energy dispersive spectroscopy (EDS-EX-250, Horiba) operated at 120 kV. The UV-visible spectra of the nanosized and nanoporous structured SnO_2 powders were obtained using a Shimadzu MPS-2000 spectrometer (Kyoto, Japan) with a reflectance sphere, over the special range of 200 to 800 nm. PL spectroscopy measurements of the nanosized and nanoporous structured SnO_2 powders were also conducted to examine the number of photoexcited electron hole pairs for all of the samples. The specific surface area is calculated according to the Brunauer-Emmett-Teller (BET) theory[11] that gives the isotherm equation for multi-layer adsorption by generalization of Langmuir's treatment of the uni-molecular layer. The BET surface area was measured using a Belsorp II-mini (BEL, Japan inc.) equipped with a TCD instrument. The pore size distribution (PDS) is an important characteristic for porous materials. Varieties of methods have been reported by researchers to identify the pore size distribution of porous materials. Among these methods, BJH and Comparison Plots[12,13] are the methods that are suitable for the range of mesopores. The relative pressure at which pore filling takes place by capillary condensation can be calculated from Kelvin's equation.[14] By using Kelvin's equation, the pore radius in which the capillary condensation occurs actively can be determined as a function of the relative pressure (P/P_0). The mean pore diameter, Dp, was calculated from $Dp = 4VT/S$, [15] where VT is the total volume of pores, and S the BET surface area.

Photocatalytic Performance of Nanoporous SnO_2. The decomposition of Bisphenol A was carried out using bed photoreactors designed in the laboratory.[16] To prepare the photodecomposition, 0.5 g of TiO_2/nanoporous SnO_2 powders (1.0:1.0 weight ratio) was added into a Pyrex cylinder reactor with 2.0 L volume. The initial concentration of Bisphenol A was 10.0 ppm/1.0 L. A UV-lamp (model BBL, 24 W/cm^2, 30 cm length × 2.0 cm diameter, Shinan Co., Korea) emitting 365 nm light was used. The Bisphenol A decomposition was performed in the condition with air bubbling. Analyses of the concentration of Bisphenol A in the reaction solution before and after the reaction were done using UV-visible spectroscopy.

Results and Discussion

Characterization of Nanoporous Structured SnO_2. Figure 1(a) shows the XRD patterns of the nanoporous structured SnO_2 powder over a long range. The specific

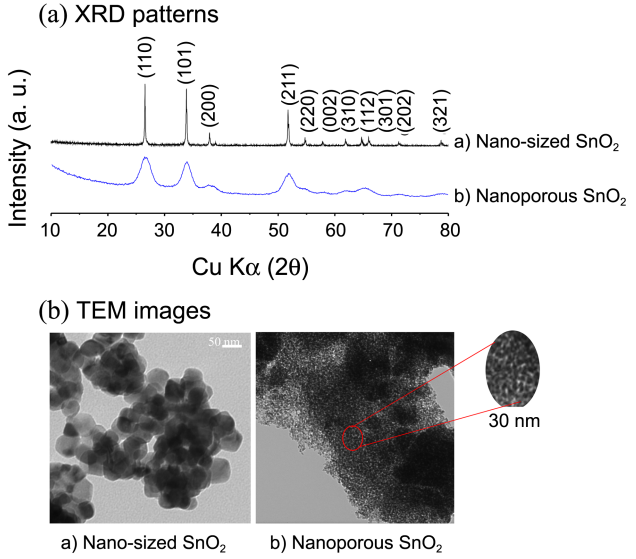

Figure 1. XRD patterns and TEM images of nanosized and nanoporous SnO_2s prepared using a conventional hydrothermal method.

peaks for the nanoporous material, MCM-41, were not observed at $2\theta = 0.98(d_{100})$, $1.62(d_{110})$, and $1.82(d_{200})$ in this study. The following lines were in good agreement with the crystalline SnO_2 standard[17] in both samples (their *hkl* indices are given in parentheses): 25.776 (110), 33.276 (101), 36.786 (200), 51.096 (211), 53.766 (220), 61.506 (310), 64.356 (301), 70.926 (202), 77.766 (321) and 83.556 (222). All of the diffraction peaks can be indexed to the tetragonal SnO_2 structure with lattice parameters a = b = 4.738 Å and c = 3.188 Å (JCPDS 041-1445). No characteristics peaks of other forms of tin oxide were detected. The full width at half maximum (FWHM) heights of the peaks at 25.8, 33.3, and 51.1° 2θ were largely broad in the nanoporous specimen compared to those of the nano-sized specimen. By Scherrer's equation,[18] the crystalline domain size was used to estimate, these which corresponded to (*d*110, 101, 211) peaks were 2.4, 3.2, and 2.1 nm for nanoporous SnO_2, respectively, compared to 52.7, 48.6, and 61.2 nm for nano-sized SnO_2, respectively. Figure 1(b) shows TEM images of the particle shape of the nanosized SnO_2, and of the pore shape and size of the nanoporous SnO_2. A relatively uniform mixture of rhombic and spherical particles whose sizes were distributed within the range of 50-60 nm was observed in the nanosized SnO_2. The nanopore sizes observed by TEM were 2.5-4.5 nm, resulted in compare to the unique hexagonal NPS used as a template, while the nanoporous SnO_2 showed irregular pore shapes.

Table 1 compares the Sn/O ratios and surface areas of the nanosized and nanoporous SnO_2 materials. First, the Sn/O ratio verse atomic percentages on the surface estimated by using EDS over the nanosized and nanoporous SnO_2 specimens were 0.31 and 0.38, respectively, which related to the lattice defects in the crystalline phase. This also indicated that the area density of Sn had greater value in nanoporous SnO_2. However, the surface area is increased for smaller

Table 1. Physical properties of nanosized and nanoporous SnO_2s prepared using a conventional hydrothermal method

Sample	Atomic composition on the surface (%)		BET surface areas (m^2/g)	Nano-pore volume (cm^3/g)	Average pore diameter (nm)
	Sn	O			
Nano-sized SnO_2	23.76	76.24	3.25	-	-
Nanoporous SnO_2	27.94	72.06	120.91	0.1573	4.53

(a) Nano-sized SnO_2

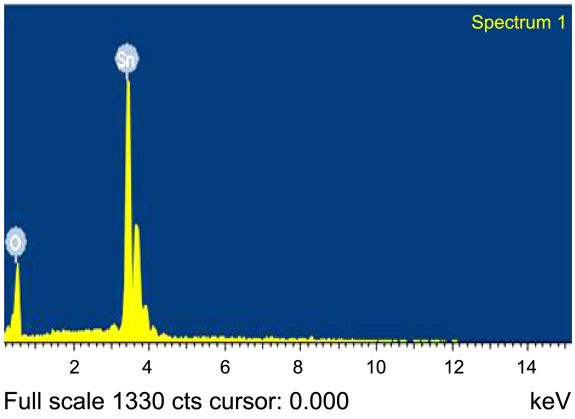

(b) Nano-sized SnO_2

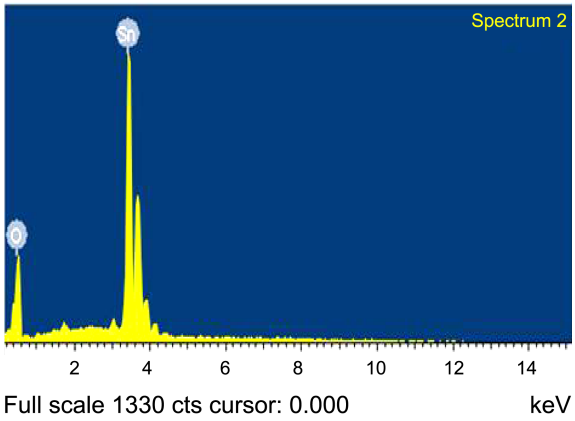

particles. The surface area of nanoporous SnO_2 (120.91 m^2/g) was larger than that of nanosized SnO_2 (3.25 m^2/g). Additionally, the nanopore volume and pore diameter in nanoporous SnO_2 were 0.16 cm^3/g and 4.53 nm, respectively. The surface area strongly affects the catalytic activity.

Figure 2(A-a) and (b) show adsorption-desorption isotherms of N_2 at 77 K for nanosized and nanoporous SnO_2, respectively. They illustrate the shape and behaviour of the N_2 adsorption isotherms for nonporous and nanoporous materials. All the isotherms belong to two types in the IUPAC classification[19]: type I at low relative pressures (P/P_0) and type IV at intermediate and high relative pressures. Type I has an important uptake at low relative pressures in both materials, characteristic of nonporous material. Particularly, the isotherms curves of adsorption and desorption were consistent in the nanosized SnO_2 material, indicating that the pore distribution could not be determined on the basis of the BJH plot, as shown in Figure 2(B-a). However, the isotherms is wide, no clear plateau is attained and a certain hysteresis slope can be observed at intermediate and high relative pressures in nanoporous SnO_2, which is indicative of the presence of large nanopores (type IV in the IUPAC classification). This was shown by the variation in the average pore diameter value, D_p, between 3.0 and 9.8 nm (Fig. 2(B-b)). The adsorption and desorption lines for nanoporous SnO_2 overlapped completely in the low relative pressure range, while the hysteresis loop was in the high relative pressure region ($P/P_0 > 0.4$), mainly due to the presence of ink-bottle types of pore.[20] These ink-bottle pore types have a larger pore size in the bottle body, which induces hysteresis in the high relative pressure region.

The UV-visible spectra of the nanosized and nanoporous SnO_2 powders were obtained to determine the band gap, as shown in Figure 3(a). The absorption band for the tetrahedral symmetry of Ti^{4+} normally appeared at a maximized 360 nm in the spectra of the nanosized TiO_2. Similar spectral responses have been reported[21] for SnO_2 and TiO_2 as both are large band gap semiconductors, although SnO_2 has a wider band gap energy (Eg) than TiO_2 (3.8 eV *vs*. 3.2 eV). The band was slightly shifted to a lower wavelength in the nanosized and nanoporous SnO_2 composites, but showed higher absorption in the TiO_2/nanoporous SnO_2 composite than in the others. The band gaps in a semiconductor material are closely related to the wavelength range absorbed, where the absorption wavelength decreases with increasing band gap. A shorter band gap eases the movement of excited electrons from the valence band to the conduction band on the surface, which occurs despite the weaker visible radiation. Otherwise, the recombination between electron and hole is faster for a smaller band gap, which decreases the photocatalytic performance. Figure 3(b) presents the PL spectra of pure TiO_2, TiO_2/nanosized and TiO_2/nanoporous SnO_2 composites. The PL curve indicates that the electrons in the valence band were transferred to the conduction band, and these excited electrons were then stabilized by photoemission. In general, if the number of the emitted electrons resulting from the recombination between excited electrons and holes is increased, the resulting increased PL intensity decreases the photoactivity. Therefore, there is a strong relationship between PL intensity and photoactivity. In particular, in the presence of a metal that can capture excited electrons or exhibit conductivity, known as the relaxation process, the PL intensity decreases to a greater extent. In this figure, the PL curve of the TiO_2/SnO_2 composite was similar to that of pure TiO_2 with an emission at 490 nm. The PL intensity of the TiO_2/nanoporous SnO_2 composite was the smallest, probably due to the action of the Sn atoms playing in capturing electron, thereby depressing the recombination process. Consequently, higher photocatalytic activities are to be expected.

Photoatalytic Efficiency on the TiO_2/Nanosized or Nano-

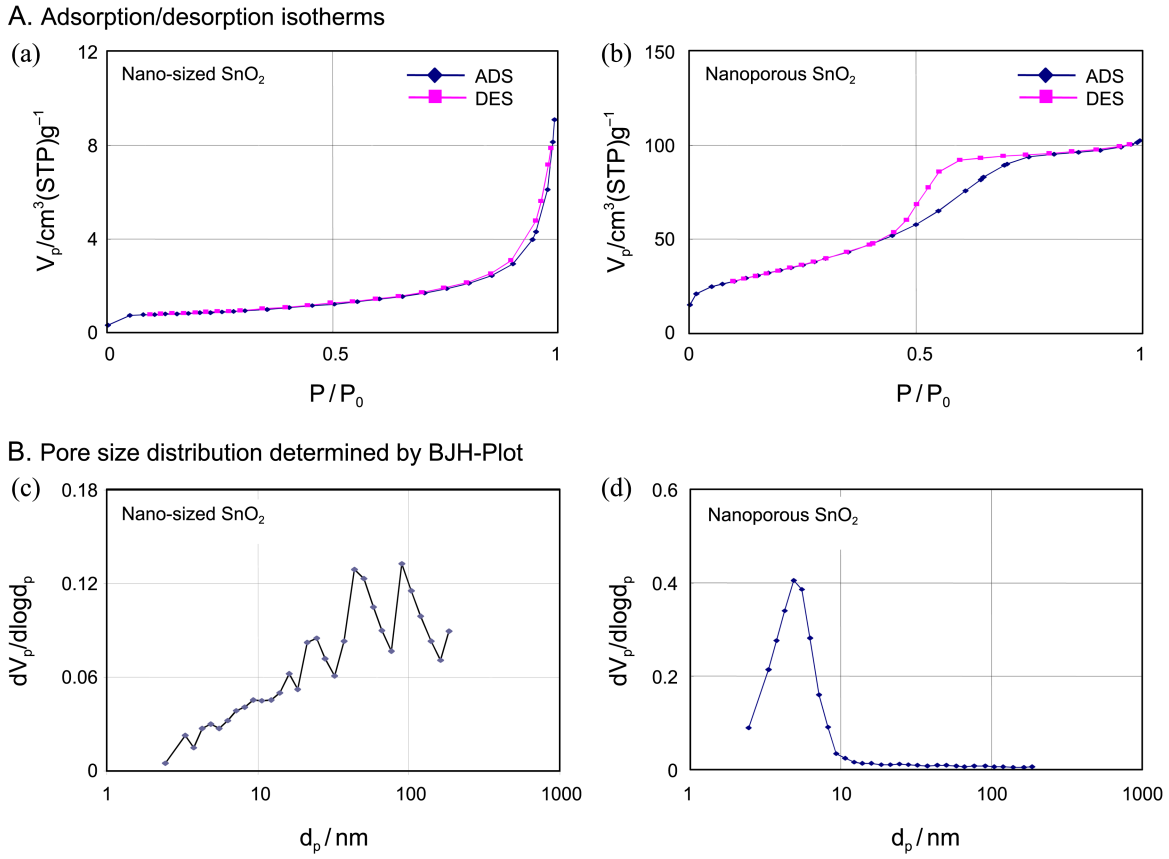

Figure 2. Adsorption/desorption isotherms and nanopore size distribution (PDS) determined by BJH plot for nanosized and nanoporous SnO_2s prepared using a conventional hydrothermal method.

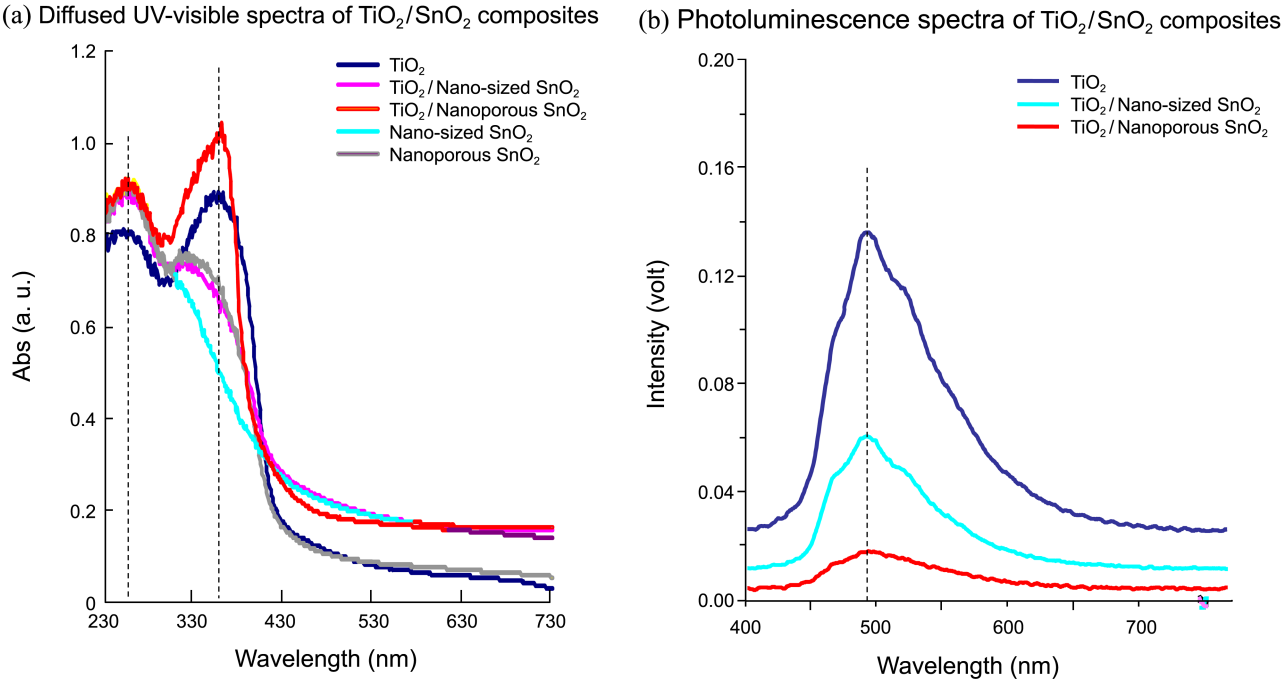

Figure 3. UV-visible and PL spectra of nanosized and nanoporous SnO_2s.

porous SnO_2 Composites. Figure 4 shows the Bisphenol A removal over TiO_2 and the TiO_2/nanosized or nanoporous SnO_2 composites. As blank Test, in the absence of light, Bisphenol A was adsorbed on the catalyst, TiO_2/nano-sized SnO_2 after 2 h, and resulted that the initial concentration of Bisphenol A was reduced to about 2%. Meanwhile, over

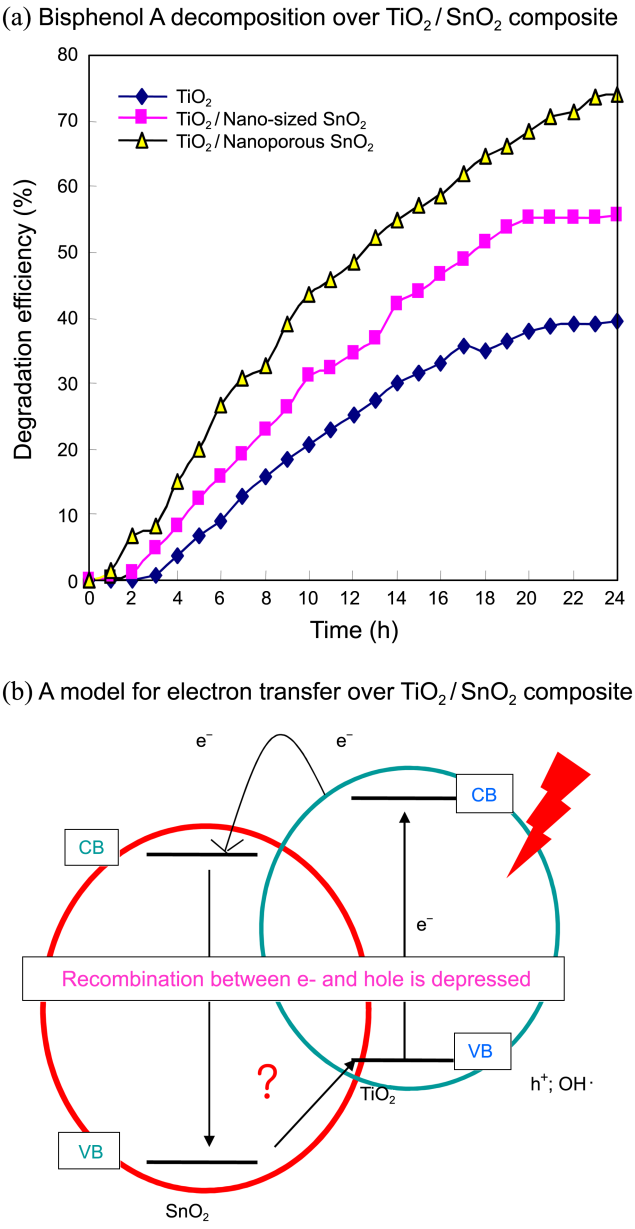

Figure 4. Comparison of photocatalytic performance of Bisphenol A over TiO_2, TiO_2/nano-sized SnO_2, and TiO_2/nanoporous SnO_2.

TiO_2/nanoporous SnO_2, the adsorption rate of Bisphenol A is faster, and 8% was adsorbed after 2 h. On the other hand, when light (365 nm) exists without catalyst, there is no concentration change of Bisphenol A until little after 2 h, however it began to decompose, and consequently the concentration of 5% decreased after 10 h. The decomposed rate was faster in the TiO_2/SnO_2 composites than in the pure TiO_2, in particular, the catalytic performance was the best over the TiO_2/nanoporous SnO_2 composite: 10.0 ppm of Bisphenol A was 75% decomposed after 24 h, while it were 20% and 40% over pure TiO_2 and the TiO_2/nanosized SnO_2 composite, respectively. This result is associated with the high surface area of nanoporous SnO_2 than can consequently adsorb a large amount of Bisphenol A and eventually dissolve much of it. The following can be correlated with the band gap. Although the band gap of SnO_2 is wider than that of TiO_2, its conduction band is at a lower energy level than that of TiO_2. As the electrical conductivity of SnO_2 is greater than that of TiO_2, the photogenerated electrons from TiO_2 in a mixture of TiO_2 and SnO_2 could be expected to be transferred easily into the SnO_2 under layer, [(TiO_2)CB $\rightarrow$ (SnO_2)CB], while the holes flow in the opposite direction into the TiO_2 over layer, [(SnO_2)VB $\rightarrow$ (TiO_2)VB], as shown in the model of Figure 4(b). Consequently, more holes reach the TiO_2 surface to be oxidized on the surface. The electrons are accumulated in the SnO_2 under layer. In addition, the photogenerated electrons from the TiO_2 conduction band may be passed to the SnO_2 conduction band or the electrons from the SnO_2 valence band may be excited to its conduction band by illumination. In conclusion, this phenomenon plays an important role in the photocatalytic performances of these type semiconductors.

Conclusions

Nanoporous SnO_2 was prepared for enhancing the photocatalytic performance for Bisphenol A destruction, and its performance was compared with that of commercial TiO_2. The pore size was 4.53 nm, as determined by BJH plot, and the surface area was 120.91 m^2/g. The following conclusions can be drawn from this study. The TiO_2/nanoporous SnO_2 composite showed better Bisphenol A destruction than TiO_2, with 10 ppm of Bisphenol A being removed 75% after 24 h. The result was attributed to the retardation of recombination between the electrons in the conduction band and the holes in the valence band over TiO_2, because the photogenerated electrons from TiO_2 in a mixture of TiO_2 and SnO_2 could be expected to be transferred easily into the SnO_2 under layer, [(TiO_2)CB $\rightarrow$ (SnO_2)CB]. To summarize, the use of nanoporous SnO_2 photocatalysts as a supplement was superior to using only pure TiO_2 material.

Acknowledgments. This work was supported by the National Research Foundation of Korea (NRF) grant funded by the Korea government (MEST) (No. 2010-0015264), for which the authors are very grateful.

References

1. Habibi, M. H.; Vosooghian, H. *J. Photochem. Photobiol. A* **2005**, *174*, 45.
2. Doh, S. J.; Kim, C.; Lee, S. G.; Lee, S. J.; Kim, H. *J. Hazard. Mater.* **2008**, *154*, 118.
3. Yoon, J.; Shim, E.; Bae, S.; Joo, H. *J. Hazard. Mater.* **2009**, *161*, 1069.
4. Daria, K.; Martin, T., Hugo, D.; Javiera, C. S. *Appl. Clay Sci.* **2009**, *42*, 563.
5. Chong, M. N.; Jin, B.; Chow, C.; Saint, C. *Water Res.* **2010**, *44*, 2997.
6. Kang, M.; Hong, W.-J.; Park, M.-S. *Appl. Catal. B* **2004**, *53*, 195.
7. Tu, Y.-F.; Huang, S.-Y.; Sang, J.-P.; Zou, X.-W. *J. Alloys Compd.* **2009**, *482*, 382.
8. Araujo, A. S.; Jaroniec, M. *Thermochimica Acta* **2000**, *363*, 175.
9. Gaydhankar, T. R.; Samuel, V.; Joshi, P. N. *Mater. Lett.* **2006**, *60*, 957.

10. Kim, W. J.; Yoo, J. C.; Hayhurst, D. T. *Micro. Meso. Mater.* **2000**, *39*, 177.
11. Rarick, R. L.; Thomas, J. J.; Christensen, B. J.; Jennings, H. M. *Advn. Cem. Bas.* **1996**, *3*, 72.
12. Esparza, J. M.; Ojeda, M. L.; Campero, A.; Herńandez, G.; Felipe, C.; Asomoza, M.; Cordero, S.; Kornhauser, I.; Rojas, F. *J. Mol. Catal. A* **2005**, *228*, 97.
13. Singh, P. S. *J. Colloid Interf. Sci.* **2008**, *325*, 207.
14. Armatas, G. S.; Petrakis, D. E.; Pomonis, P. J. *Micro. Meso. Mater.* **2005**, *83*, 251.
15. Díaz-Díez, M.A.; Gómez-Serrano, V.; Fernández González, C.; Cuerda-Correa, E. M.; Macías-García, A. *Appl. Surf. Sci.* **2004**, *238*, 309.
16. Yeo, M.-K.; Kang, M. *Water Res.* **2006**, *40*, 1906.
17. Chang, S.-S.; Yoon, S. O.; Park, H. J. *Ceramics Inter.* **2005**, *31*, 405.
18. Houšková, V.; Štengl, V.; Bakardjieva, S.; Murafa, N. *J. Phys. Chem. Solids* **2008**, *69*, 623.
19. Khalfaoui, M.; Knani, S.; Hachicha, M. A.; Lamine, A. B. *J. Colloid Interf. Sci.* **2003**, *263*, 350.
20. Chieh, C. C.; Chon, K. *J. Catal.* **1970**, *17*, 71.
21. Shifu, C.; Lei, C.; Shen, G.; Gengyu, C. *Mater. Chem. Phys.* **2006**, *98*, 116.